Optical activity of a single MnAs cluster: Birefringence or Kerr effect

M. Leuschner[a], P.J. Klar[a,*], W. Heimbrodt[a], W.W. Rühle[a], S. Hara[a,b,1], W. Stolz[a], K. Volz[a], T. Kurz[c], A. Loidl[c], H.-A. Krug von Nidda[c]

[a]*Department of Physics and Material Sciences Center, Philipps University, Renthof 5, 35032 Marburg, Germany*
[b]*Fujitsu Laboratories Ltd., 10-1 Morinosato-Wakamiya, Atsugi 243-0197, Japan*
[c]*Experimentalphysik V, Elektronische Korrelationen und Magnetismus, Institut für Physik, Universität Augsburg, 86135 Augsburg, Germany*

*Corresponding author. Tel.: +49 0 6421 2821354; fax: +49 0 6421 2827036.
E-mail address: peter.klar@physik.uni-marburg.de (P.J. Klar).
[1]Present address: Graduate School of Information Science and Technology, Hokkaido University, North 14 West 9, Sapporo 060-0814, Japan.

1. Introduction

Semiconductor-based granular ferromagnetic–paramagnetic hybrid systems have recently attracted much attention [1–16]. These hybrid structures usually consist of a paramagnetic semiconductor matrix such as GaAs:Mn where ferromagnetic inclusions such as MnAs are incorporated.

The reasons for the considerable interest in these materials are manifold. First, these hybrids exhibit large negative and positive magneto-resistance effects whose origin is still not entirely understood [8,9,12,14]. Examples are current studies of the magneto-resistance behavior of GaAs:Mn/MnAs [8,9,4,14], of GaAs:Er/ErAs [10], of GaAs:Mn/MnSb [11], or of Ge:Mn/$Mn_{11}Ge_8$ [12]. Understanding and optimizing these effects might yield new semiconductor-based magneto-electronic devices.

Second, several studies of GaAs:Mn/MnAs hybrids and optical semiconductor devices containing this hybrid exhibit giant magneto-optical effects which raise expectations that such hybrids are applicable in magneto-optical devices (e.g. optical isolator structures) in photonic integrated circuits (PICs) [2,4,16–18]. A major advantage of the III-V based magnetic hybrid structures is that they can be monolithically combined with the present PICs fabricated of III-V compound semiconductors. InP-related materials form the basis for highly integrated PICs for optical communication systems. The granular $In_{0.54}Ga_{0.46}As$:Mn/MnAs hybrid studied here is compatible with InP technology [16].

The ferromagnetic clusters embedded in the matrix material are the source of the optical activity of these magnetic hybrid structures. Therefore, the study of the properties of a single ferromagnetic cluster is of interest. Usually the crystal symmetry of the ferromagnetic inclusions is rather low resulting in an optical anisotropy which leads to an optical activity of non-magnetic origin (such as linear birefringence) in addition to magneto-optical activity (such as Kerr or Faraday effect) due to the spontaneous magnetization.

The cluster diameters as well as the spacing between clusters are typically below 100 nm. Therefore, the spatial resolution achievable by most conventional optical microscopic techniques is not sufficient to resolve individual clusters. This problem can be overcome by using experimental set-ups for scanning near-field optical microscopy (SNOM). A variety of SNOM-based measurements of the optical properties of small magnetic structures such as magnetic domains [19–22] or artificial mesoscopic magnetic nanostructures [23,24] have been discussed and performed. "SNOM based methods" in the sense that for studying far-field effects such as linear Kerr, Faraday or birefringence effects (which are the properties of interest of the optically active layers in PICs) one only makes use of the high spatial resolution achievable with SNOM techniques but tries to avoid near-field effects. This is usually done by illuminating the sample via the SNOM tip and detecting in the far-field using a microscope objective in reflection or transmission geometry [19,24]. Most linear optical processes of non-magnetic origin leading to optical activity (including most of the near-field optical effects) exhibit time-reversal symmetry in contrast to the magneto-optical effects which break time-reversal symmetry. A Sagnac interferometer in conjunction with a SNOM system makes use of this fact. Such a set-up is sensitive only to processes contributing to the optical activity which break the time-reversal symmetry. Therefore, it can be used to measure magneto-optical effects even when operating with near-field illumination and detection [21,23].

Here, we employ a depolarization reflection SNOM set-up with uncoated fiber probe-tips, which was pioneered by von Freymann et al. [25–27]. We study the optical activity of single ferromagnetic MnAs clusters embedded in a paramagnetic $In_{0.54}Ga_{0.46}As$:Mn matrix. The distance between the sample and the probe tip has to be chosen such that near-field effects are minimized, whilst retaining a sufficient spatial resolution to resolve individual MnAs clusters, as the same fiber tip is used for illumination and detection. The optical activity of a single cluster measured in this type of reflection experiment results from contributions due to birefringence and Kerr effect. We have also performed angle-dependent

ferromagnetic resonance (FMR) measurements of the sample to correlate the observed optical activity with the structural and magnetic properties of the MnAs clusters. The properties of the spontaneous magnetization of the clusters with respect to the hexagonal crystal structure of the cluster itself as well as the predominant cluster orientations with respect to the surrounding zincblende matrix are thus identified [14,28]. Finally, we estimate the relative magnitude of the birefringence and the polar Kerr effect.

2. Sample preparation and characterization methods

The hybrid structure consisting of a paramagnetic $In_{0.54}Ga_{0.46}As$:Mn matrix and ferromagnetic MnAs clusters was grown by metal–organic vapor-phase epitaxy (MOVPE). The layers were grown on InP (1 0 0) substrates at a growth temperature of 590 °C using tertiarybutylarsine, triethylgallium, trimethylindium, and bis-(methylcyclopentadienyl)manganese as precursors. The nominal Mn/(III + Mn) ratio was 0.24 in the gas phase. Further details of the sample growth are given in Ref. [16]. Hexagonal MnAs clusters are formed within the $In_{0.54}Ga_{0.46}As$:Mn matrix with Mn-doping levels of about $10^{19}\,cm^{-3}$ under these growth conditions. The crystallographic *c*-axis of the MnAs clusters is always in a good approximation parallel to one of the ⟨1 1 1⟩ directions of the zincblende matrix similar to MnAs clusters formed in GaAs:Mn [29].

Fig. 1 shows an atomic force microscopy (AFM) image of the surface of the $In_{0.54}Ga_{0.46}As$:Mn/MnAs hybrid sample. The clusters, which are always formed close to the surface of the layer, can be clearly seen. The clusters have a cone shape and are elongated towards the [0 1 1] direction of the zincblende matrix. The clusters either stand out of the matrix or are embedded in valleys in the matrix. The lateral dimensions of the clusters are of the order of 150 nm and about 4% of the surface are covered with clusters. The surface of the surrounding $In_{0.54}Ga_{0.46}As$:Mn matrix is very flat, i.e. monoatomic surface steps can be clearly distinguished in the AFM image.

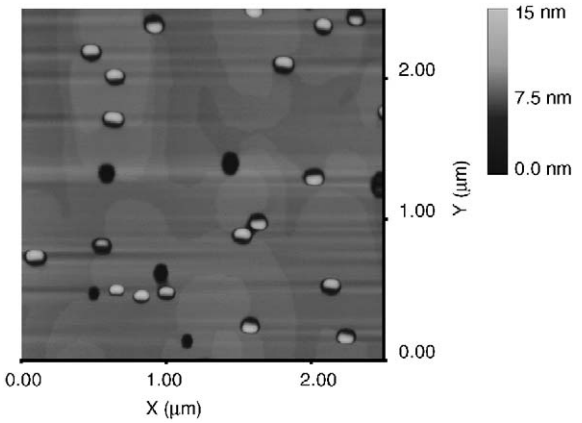

Fig. 1. AFM image of the surface of the $In_{0.54}Ga_{0.46}As$:Mn/MnAs sample.

The ferromagnetic properties of the MnAs clusters were studied by SQUID and FMR measurements. SQUID magnetization measurements revealed that the hybrid sample exhibits a Curie temperature of $T_C \approx 320\,K$. The FMR measurements were performed at 150 K using a Bruker ELEXSYS E500 CW-spectrometer at X-band frequency ($\nu \approx 9.35\,GHz$), equipped with a continuous gas-flow He cryostat. The FMR spectra record the power P_{abs} absorbed by the sample from the transverse magnetic microwave field as a function of the static magnetic field H. The signal-to-noise ratio of the spectra is improved by detecting the derivative dP_{abs}/dH using a lock-in technique with 100 kHz field modulation. The sample was glued on a suprasil–quartz rod, which allowed the rotation of the sample around defined crystallographic axes.

The optical and magneto-optical properties of single MnAs clusters were probed using a SNOM set-up. Fig. 2 depicts schematically the experimental set-up for the depolarization SNOM measurements. The linearly polarized light of a HeNe laser (632.8 nm) is coupled into an optical fiber via a beam splitter and a microscope objective. Several loops in the fiber act as a polarization control. The left and the right loop are single loops serving as quarter-wave plates allowing one to compensate the depolarization of the laser light in the optical fiber due to the

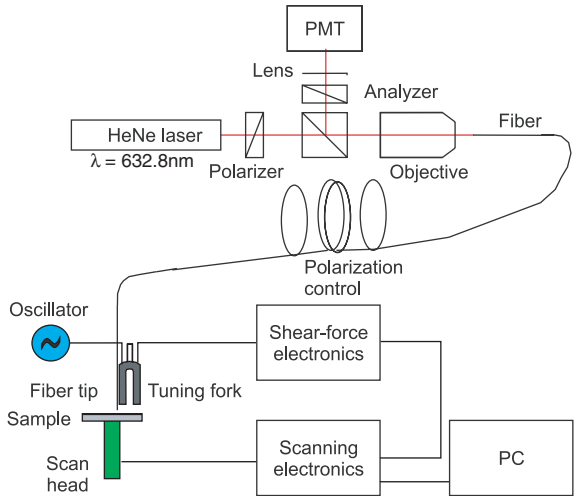

Fig. 2. Schematic diagram of the experimental set-up for depolarization SNOM measurements.

bending of the fiber. The center loop is a double loop acting as a half-wave plate and is used for adjusting the polarization plane. The laser light passes through the optical fiber up to the probe tip which is connected to the sampling head. The light emitted by the probe tip is reflected by the sample. The reflected light is recollected by the same tip and traverses the same fiber and microscope objective in the opposite direction. The reflected light is detected with a photomultiplier after passing the beam splitter and another linear polarizer serving as an analyzer. The distance between probe tip and sample surface is controlled within a few nanometers by tracing the shear force on the tip which is glued to a tuning fork piezo [30]. The sample is mounted on a scan head with *xyz*-movement which is positioned by commercial scanning electronics. Scans were acquired in the constant distance mode (CDM) as well as in the constant height mode (CHM). The CHM scans were performed for various relative positions of the polarizer and analyzer.

In the CDM, the distance between the probe tip and the sample surface is typically in the range of 5 to 10 nm whereas, in the CHM, this distance is usually much bigger. We typically operated with a distance of about 100 nm between the mean position of the sample surface and the probe tip yielding a spatial resolution of about 250 nm. Near-field effects are minimal at this rather large distance, being essential in our study of the far-field effects such as birefringence and Kerr effect. All measurements were performed at 20 °C, i.e. below the Curie temperature of the MnAs clusters.

3. Measurement of the magnetic properties of the MnAs clusters

The FMR approach employed here to identify the magnetic properties of the ferromagnetic MnAs clusters is described in detail in Ref. [28] where the related granular hybrid GaAs:Mn/MnAs was studied successfully and where it was shown that angular dependent FMR measurements at a constant temperature below the Curie-temperature of the MnAs clusters reveal the magnetic anisotropy of the clusters. The observed anisotropy of the ferromagnetic resonance field can be described theoretically and correlated with the MnAs clusters using a model for the ferromagnetic resonance condition based on the Smith–Suhl formula accounting for the Zeeman effect, magneto-crystalline anisotropy and demagnetization effects. The properties of the spontaneous magnetization of the MnAs clusters with respect to the hexagonal crystal structure of the cluster itself as well as the predominant cluster orientations with respect to the surrounding zincblende $In_{0.54}Ga_{0.46}As$:Mn matrix can be determined in this fashion.

An appropriate overview of the angular dependence of the FMR spectra is achieved by a two-dimensional map in grey scale of the FMR signal in dependence on magnetic field and rotation angle. The bright regions denote values larger than zero, whereas the dark regions indicate values below zero. Hence, the resonance field is located approximately in the middle between bright maximum and dark minimum. The FMR signals show a strong angular dependence due to the uniaxial symmetry of MnAs. The two frames in Fig. 3 show the rotation patterns of the $In_{0.54}Ga_{0.46}As$:Mn/MnAs sample under study, where the rotation axis has been chosen along the [0 1 −1] and [0 1 1] direction, respectively. The

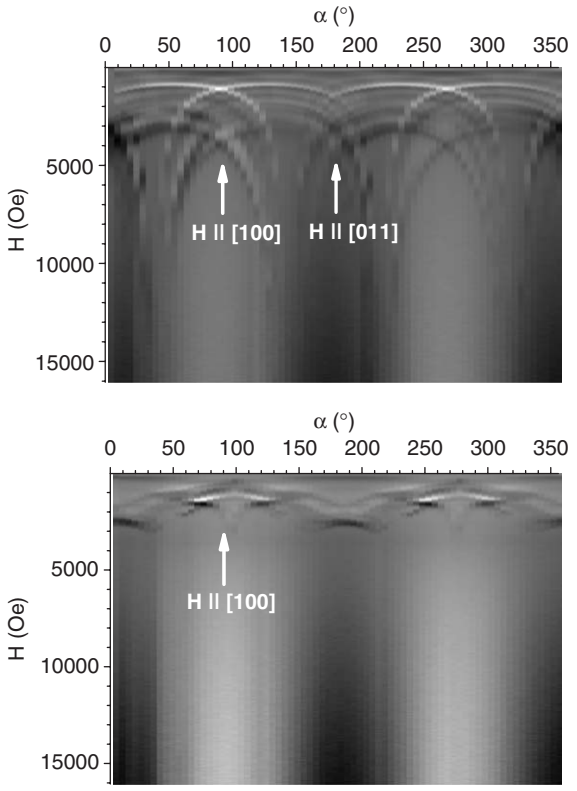

Fig. 3. Two-dimensional grey-scale maps of the angular dependence of the ferromagnetic resonance of the $In_{0.54}Ga_{0.46}As$:Mn/MnAs hybrid sample for different rotation axes. Upper frame: rotation about the zincblende [0 1 −1] direction. Lower frame: rotation about the zincblende [0 1 1] direction. $T = 150\,K$.

FMR pattern is dominated by two coexisting curves with a period of 180° and with their minimum resonance field near 1 kOe for rotation about the [0 1 −1] axis. This double pattern is indicative for the co-existence of two subensembles of MnAs clusters with their hexagonal axis along the (In,Ga)As [1 1 1] and [−1 1 1] direction, respectively. The angle dependence also reveals that the *c*-axis of the clusters is the hard magnetization axis and the basal plane serves as an easy plane for the magnetization. The resonance signals in the second grey-scale map in the lower frame of Fig. 3 are much weaker than in the upper frame, meaning that there are hardly any MnAs clusters present in the sample with their *c*-axes oriented along [1 1 −1] and [1 −1 1]. A signal becomes visible only when the magnetic field is applied perpendicular to the film plane. This is an effect which arises again from the MnAs clusters oriented along the (In,Ga)As [1 1 1] and [−1 1 1] axes. The signals sum up most effectively for this orientation, whereas for other orientations the signals are smeared out due to the finite distribution of the cluster axes and shapes.

4. Measurement of the optical activity of the MnAs clusters

Fig. 4 shows the results of SNOM scans of the surface of the granular $In_{0.54}Ga_{0.46}As$:Mn/MnAs sample obtained in the CDM (top and center) and in the CHM (bottom). The top image is an *xy*-plot of the movement of the *z*-piezo element in the CDM derived from the control voltage applied to the *z*-piezo element to maintain a constant shear-force on the probe tip. Such a topography plot of the sample surface is comparable to the AFM image in Fig. 1. The black features are due to the MnAs clusters. They appear to be embedded in valleys on the sample surface which are about 5 nm deep and about 90 nm wide. These findings are somewhat in contrast to those of the AFM image where the clusters were found to stand out of the sample surface as well as to be situated in valleys. This difference probably arises from a material contrast in the SNOM topography which originates from a different functional dependence of the shear force on the distance from the surface for MnAs and for (In,Ga)As:Mn. The white spot in the image is due to a dust particle on the sample surface. The lateral as well as the vertical spatial resolution is not as good as in the AFM image, mainly because the radius of the SNOM tip is larger than that of a typical AFM tip.

The lower two images are a comparison of intensity *xy* scans of the reflected light obtained in the CDM and the CHM. The CDM image was obtained with crossed polarizers whereas the CHM image was acquired with parallel polarizers. MnAs clusters on the sample are clearly observed as dark features in the CHM image. The correspondence between the features in the topographic image and the CHM image is obvious. The MnAs

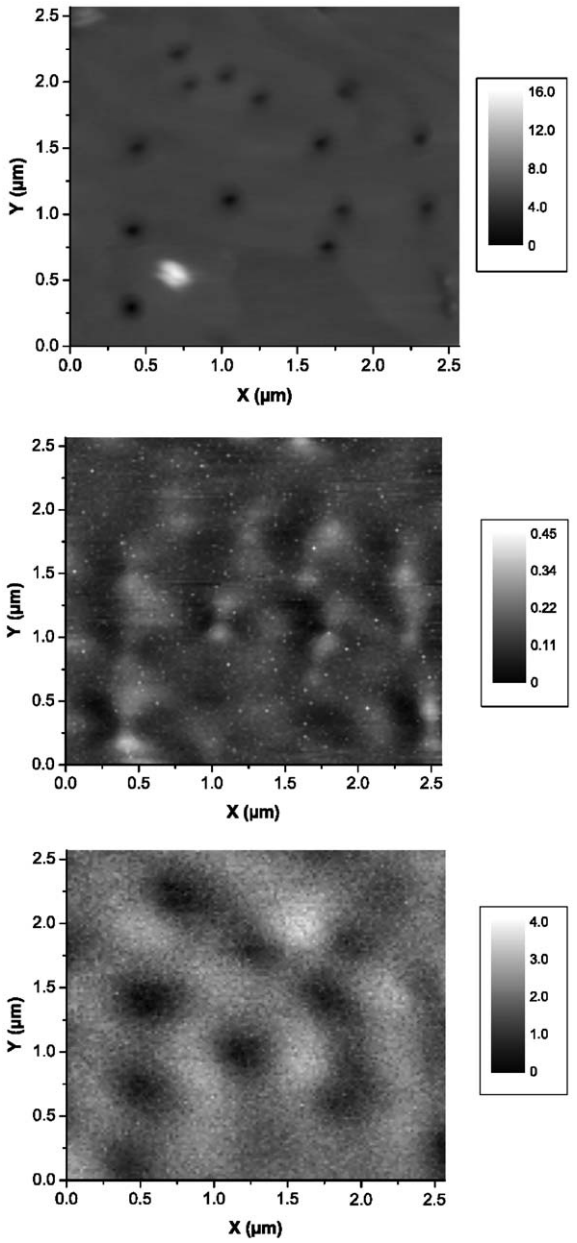

Fig. 4. Comparison of scans of the topography (top), the corresponding constant distance mode (center) and constant height mode signals (bottom) of the surface of the $In_{0.54}Ga_{0.46}As$:Mn/MnAs sample. The topography is recorded via the calibrated control voltage applied to the z-piezo element to maintain a constant shear-force on the probe tip. The CDM and the CHM signals were recorded for crossed (90°) and parallel (0°) polarization directions of polarizer and analyzer, respectively.

cluster-related features in the CHM image are somewhat blurred compared to those in the topographic image because of the divergence of the probe light emitted by the tip when traversing the relatively large distance of 100 nm to the sample surface and back. Nevertheless, these measurements clearly indicate that the spatial resolution under these operating conditions of the SNOM set-up even for distances of about 100 nm between the probe tip and the sample is sufficient for resolving individual MnAs clusters and, thus, for probing a single MnAs cluster. The center image in the CDM shows no improvement in resolving the MnAs clusters despite the much smaller average distance between tip and sample surface. The reason is that, at these shorter distances, a larger amount of topography-induced multi-scattered light is collected by the tip in addition to the singly reflected light. These topography-induced effects make the interpretation of the CDM images very difficult. Furthermore, we must avoid near-field effects when studying the far-field birefringence and Kerr effect of the MnAs clusters. Therefore, we will focus in the following on images obtained in the CHM.

Fig. 5 shows three CHM scans of the surface of the $In_{0.54}Ga_{0.46}As$:Mn/MnAs sample for three different angles between the polarization directions of incoming light and the detected light reflected from the sample surface. The angles between the polarization direction of the polarizer and the analyzer were 85°, 90°, and 95° in the upper, center, and bottom image, respectively.

Let us first compare the CHM scans with parallel and crossed polarizations, i.e. the bottom image in Fig. 4 and the center image in Fig. 5, respectively. Both images clearly show the clusters and the surrounding matrix. It can be seen that the contrast is almost entirely inverted, i.e., in the CHM image for parallel polarizations the clusters appear as dark spots in a bright matrix whereas in the CHM image for crossed polarizations the situation is vice versa. This is already a strong indication that the observed contrast arises from differences in the optical activity of matrix and clusters and not from differences in absorption. For dominant absorption, one would expect the same contrast in both images. The CHM image for

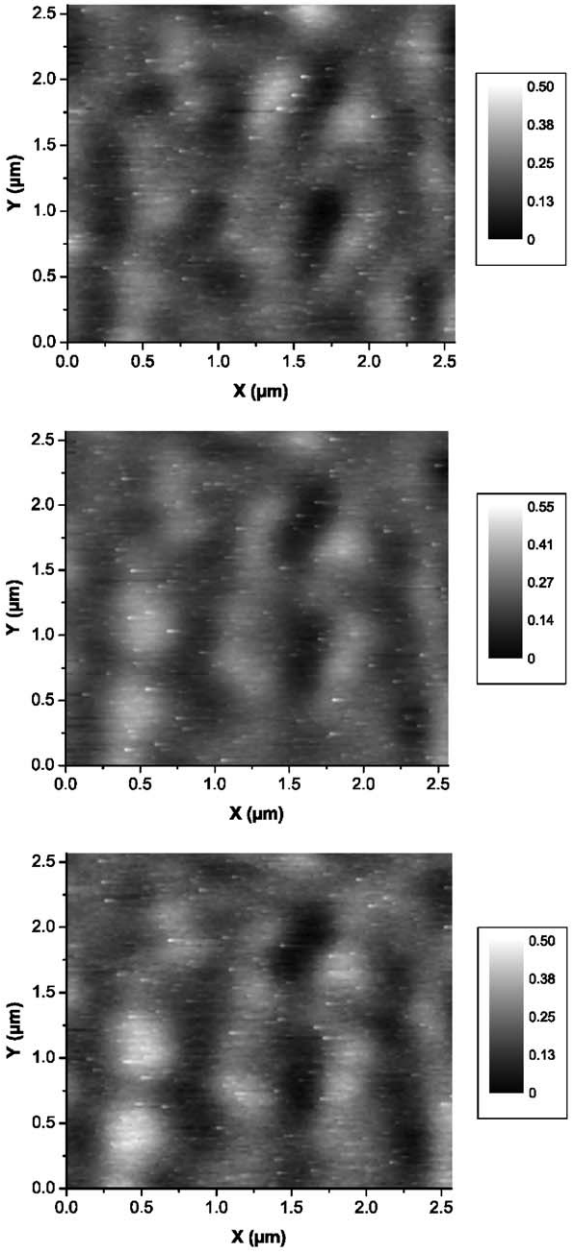

Fig. 5. Constant height mode scans of the surface of the $In_{0.54}Ga_{0.46}As$:Mn/MnAs sample for three different angles between the polarization directions of polarizer and analyzer. Top: 85°; center: 90° (i.e. crossed polarizers); bottom: 95°.

the parallel configuration appears less blurred than that acquired with crossed polarizers since the signals are about a factor of 50 stronger in the former case and since the signal-to-noise ratio increases with decreasing signal strength. The contrast ratio for both images is about 1:1.4.

We will now compare the three CHM images in Fig. 5 obtained in the vicinity of the crossed polarization configuration. In both, the upper and the lower, CHM images the relative angle between the polarization directions of the polarizer and the analyzer was varied only by 5° with respect to the crossed polarizer position. If the optical activities of the cluster and the matrix were zero one would expect that the two images showed the same contrast. This is clearly not the case. The CHM image for the polarizer–analyzer angle of 95° shows a higher contrast than that obtained for an angle of 85°. Indeed the contrast increases varying the angle from 85° via 90° to 95°. This is another clear indication that the clusters are optically active.

Fig. 5 also shows that the contrast is enhanced in almost the same way for all the clusters, which can be further corroborated by analyzing the intensity of the reflected light as a function of polarizer–analyzer angle for the MnAs clusters with respect to a reference point on the $In_{0.54}Ga_{0.46}As$:Mn matrix. Exemplarily, the top graph of Fig. 6 shows a comparison of the dependence of the reflected intensity on the polarizer–analyzer angle α for an individual MnAs cluster and the $In_{0.54}Ga_{0.46}As$:Mn matrix. The experimental data points are fitted by the theoretically expected $\cos^2\alpha$-dependence. The angular shift $\Delta\alpha$ of 1.64° between the two curves is indicative for the difference in optical activity of the $In_{0.54}Ga_{0.46}As$:Mn matrix and the MnAs cluster. This analysis has been performed for 14 796 different scan positions of the CHM images obtained for different polarizer–analyzer positions with respect to a typical position on the MnAs matrix. The resulting frequency-rank distribution is shown in the lower graph of Fig. 6. The main peak centered at $\Delta\alpha \approx 0°$ arises from positions on the $In_{0.54}Ga_{0.46}As$:Mn matrix. The smaller peak centered at $\Delta\alpha \approx 1.4°$ is due to the MnAs clusters. The magnitudes of the two peaks simply reflect that only 4% of the scanned sample surface are covered with MnAs clusters, as a consequence, the $\Delta\alpha$ peak due to the MnAs clusters is only just

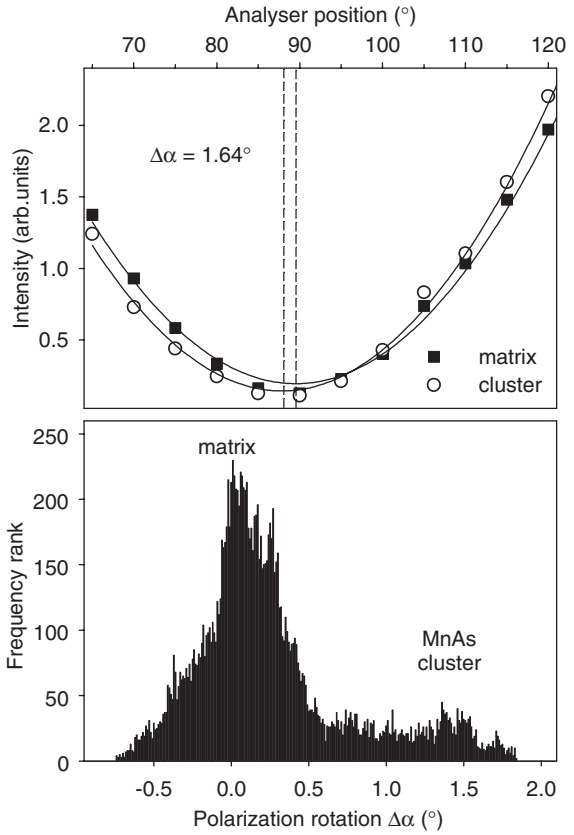

Fig. 6. Top: Intensity of the reflected light as function of angle between the polarization directions of the polarizer and the analyzer (0° and 90° correspond to parallel and crossed polarizations, respectively) for stationary tip positions on the $In_{0.54}Ga_{0.46}As$:Mn matrix and a MnAs cluster, respectively. Bottom: Frequency-rank distribution of the observed angular shift $\Delta\alpha$ with respect to fixed (typical) matrix position. 117×128 positions of the *xy* scans were evaluated.

distinguishable above the noise level in the frequency-rank distribution. The asymmetric shape of the $\Delta\alpha$ peak is interesting. The shoulder towards lower angles probably corresponds to positions in matrix regions between MnAs clusters where the clusters are close to each other (see lower image of Figs. 4 and 5). We cannot presently decide whether this is due to a Kerr effect in the paramagnetic matrix induced by the dipolar stray-field of the ferromagnetic cluster or a topography-induced effect.

5. Optical activity in terms of birefringence and Kerr effect

The $In_{0.54}Ga_{0.46}As$:Mn matrix has to a first approximation a cubic zincblende structure since biaxial strain due to lattice mismatch between the hybrid layer and the InP substrate as well as inhomogeneous strain fields due to the clusters are negligible. Therefore, the refractive index is isotropic ruling out any birefringence in the matrix. Furthermore, the spontaneous magnetization of the paramagnetic $In_{0.54}Ga_{0.46}As$:Mn matrix is zero to a first approximation because the magnetic moments of the Mn ions are randomly oriented in absence of an external magnetic field when dipolar stray-fields of the MnAs clusters are neglected. This also rules out the occurrence of a Kerr effect in the matrix material. Therefore, the $In_{0.54}Ga_{0.46}As$:Mn matrix is optically inactive. In contrast, MnAs is a uniaxial crystal as well as a ferromagnet at room temperature. In conclusion, the observed difference between the optical activity of the MnAs clusters and that of the $In_{0.54}Ga_{0.46}As$:Mn matrix must be entirely due to birefringence and Kerr effect of the MnAs clusters. The observed rotation of the polarization can then be written as the sum of the two contributions:

$$\Delta\alpha = \Phi_{\mathrm{Kerr}} + \Phi_{\mathrm{birefringence}}. \tag{1}$$

Let us first consider the contribution of the Kerr effect. At normal incidence, only the polar Kerr effect (due to the component of the magnetization perpendicular to the surface, i.e. parallel to the [1 0 0] direction of the matrix) yields a non-zero rotation of the polarization (see e.g. Ref. [32]) which is given by

$$|\Phi_{\mathrm{Kerr}}| = \left|\mathrm{Im}\left(\frac{\tilde{n}\tilde{Q}}{\tilde{n}^2-1} \times \frac{|\vec{M}_{[1\,0\,0]}|}{|\vec{M}|}\right)\right|, \tag{2}$$

where $\tilde{n} = n(1 - ik)$ is the complex refractive index and $\tilde{Q} = Q_0 \exp(-q)$ is the complex magneto-optical constant. Q_0 and q are denoted as Voigt parameters. We estimate $|\Phi_{\mathrm{Kerr}}| < 0.05°$ using the parameters determined by Stoffel and Schneider for 633 nm in a longitudinal Kerr-rotation experiment on MnAs films [33]. The $\vec{M}_{[1\,0\,0]}$ is the

projection of the magnetization $\vec{M}$ of the MnAs cluster onto the [1 0 0] direction. We do not distinguish between ordinary and extraordinary complex refractive index (see discussion of the birefringence below) in this discussion of the Kerr rotation, since it does not affect the estimate of the order of magnitude of Φ_{Kerr}. The values for n and k determined by Stoffel and Schneider most likely correspond to the ordinary refractive index. Our estimate of the Kerr rotation is comparable to other Kerr measurements on MnAs at various wavelengths and geometries [33–35]. We conclude that the Kerr effect alone does not explain the experimentally observed rotations of the polarization ranging from $\Delta\alpha \approx 1.3^\circ$ to 1.7°.

We will now estimate the magnitude of the birefringence. The refractive index of MnAs will be different along the c-axis and in the basal plane because of the hexagonal symmetry of the MnAs clusters, i.e. hexagonal MnAs is a uniaxial crystal. The incoming linearly polarized light propagates along the [–1 0 0] direction of the matrix. The c-axis of the MnAs (parallel either to the [1 1 1] or the [–1 1 1] direction of the zincblende matrix) and the propagation direction of the incoming light form the principal plane, the (0 1 –1) plane for both cluster orientations. The incoming light with electric field vector $\vec{E}_{\mathrm{i}}$ can be divided into two components, the ordinary beam (whose electric field vector $\vec{E}_{\mathrm{i}}^{\mathrm{o}}$ is normal to the principal plane) and the extraordinary beam (whose electric field vector $\vec{E}_{\mathrm{i}}^{\mathrm{e}}$ lies within the principal plane). The complex refractive index of the ordinary beam $\tilde{n}_{\mathrm{o}}$ does not depend on the propagation direction, whereas that of the extraordinary beam component depends on the angle Θ_c between the propagation direction of the light and the c-axis:

$$\tilde{n}_{\mathrm{e}}(\Theta_c) = \tilde{n}_{\mathrm{o}} \sqrt{\frac{1+\tan^2\Theta_c}{1+(\tilde{n}_{\mathrm{o}}/\tilde{n}_{\mathrm{e}})^2\tan^2\Theta_c}}, \tag{3}$$

where $\tilde{n}_{\mathrm{e}}$ is the complex refractive index when the propagation direction of the light is in the principal plane, but perpendicular to the c-axis. In the particular geometry of the SNOM experiment, the principal plane as well as the angle $\Theta_c = 54.7^\circ$ are the same for both orientations of the MnAs c-axis found in the FMR experiment.

The reflection coefficients at normal incidence for $|\vec{E}_{\mathrm{i}}^{\mathrm{o}}|^2$ and $|\vec{E}_{\mathrm{i}}^{\mathrm{e}}|^2$ of the incoming light are given by

$$R^{\mathrm{o}} = \left|\frac{(\tilde{n}_{\mathrm{o}}-1)^2}{(\tilde{n}_{\mathrm{o}}+1)^2}\right| \quad \text{and} \quad R^{\mathrm{e}}(\Theta_c) = \left|\frac{(\tilde{n}_{\mathrm{e}}(\Theta_c)-1)^2}{(\tilde{n}_{\mathrm{e}}(\Theta_c)+1)^2}\right|, \tag{4}$$

respectively. The polarization rotation $\Delta\alpha$ of the electric field vector $\vec{E}_{\mathrm{r}}$ of the reflected light with respect to $\vec{E}_{\mathrm{i}}$ can be calculated as

$$\Phi_{\mathrm{birefringence}} = \alpha - \arctan\left(\sqrt{\frac{R^{\mathrm{o}}}{R^{\mathrm{e}}(\Theta_c)}}\tan\alpha\right), \tag{5}$$

if we define α as the polarization angle between polarization vector $\vec{E}_{\mathrm{i}}$ of the incoming light and the projection of the c-axis onto the (1 0 0) plane.

To our knowledge, no experimental data are available for the ordinary and extraordinary complex refractive indices of MnAs at 633 nm. Therefore, we proceed as follows. We assume that the ordinary refractive index is given by $\tilde{n}_{\mathrm{o}} = n - ik$, where $n = 2$ and $k = 1.2$ are taken from the experimental work of Stoffel and Schneider [33]. A value of $R^{\mathrm{o}} = 0.47$ (where $\vec{E}_{\mathrm{i}} \perp c$) is obtained in agreement with the theoretical values from Fig. 5 of Ref. [36]. A reflectivity $R^{\mathrm{e}} = 0.6$ (where $\vec{E}_{\mathrm{i}} \| c$) [36] yields $\tilde{n}_{\mathrm{e}}$ assuming $\tilde{n}_{\mathrm{e}} = (n + \Delta n)(1 - ik)$. A $\Delta n = 1.15$ is finally obtained.

The birefringence-induced polarization rotation $\Phi_{\mathrm{birefringence}}$ calculated with Eqs. (3)–(5) using these values is plotted versus α in Fig. 7. The observed $\Delta\alpha$ values of the MnAs clusters of 1.3° to 1.7° lie in the range of the calculated birefringence-induced polarization rotation angles. Unfortunately, an accurate measurement of the angle dependence $\Delta\alpha$ versus α as well as of α itself was not feasible with our experimental SNOM set-up, therefore, we have to refrain from a more detailed quantitative analysis.

The polarization rotation angles due to the magneto-optical Kerr effect discussed above are about one order of magnitude smaller than the experimental value suggesting that the experimentally observed rotation of the polarization is almost entirely determined by birefringence. This minor contribution of the Kerr effect is further

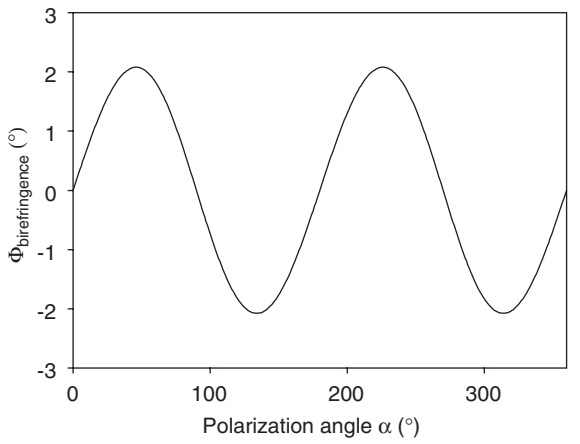

Fig. 7. Calculated rotation angle of the polarization rotation of light reflected from a uniaxial MnAs cluster as a function of the polarization direction of the incoming light. The uniaxial *c*-axis of the MnAs cluster is assumed to be parallel to the [1 1 1] direction of the $In_{0.54}Ga_{0.46}As$:Mn matrix and the propagation direction of the incoming (reflected) light is antiparallel (parallel) to the [1 0 0] direction of the matrix. In this geometry the angle between the uniaxial *c*-axis and the propagation directions of the incoming and reflected light is 54.7°. The analyzer position is defined as the angle between the polarization direction of the incoming light and the [0 1 1] direction, i.e., the direction of the projection of the *c*-axis on to the (1 0 0) plane.

corroborated by the fact that all the clusters basically exhibit the same optical activity $\Delta\alpha$ (see Fig. 5). Such a behavior is expected if the uniaxial crystal symmetry of the MnAs determines the optical activity because then all the clusters (i.e. both cluster orientations determined in the FMR experiment) should behave in the same way. This result delivers another argument against the Kerr effect being of importance of the observed optical features: The projection of the cluster magnetization $\vec{M}$ onto the propagation direction of the light determines the magnitude of the Kerr effect. In the absence of an external magnetic field, the magnetization of a MnAs cluster has a random orientation in the basal plane of the hexagonal lattice. The projections $\vec{M}_{[1\,0\,0]}$ onto the [1 0 0] direction for different clusters might range in this case between $-0.82 \times |\vec{M}|$ (for $\vec{M}$ along [−2 1 1]) and $0.82 \times |\vec{M}|$ for $\vec{M}$ along [2 −1 −1]. The corresponding Kerr-rotation angle of the polarization should vary accordingly as the polar Kerr effect is proportional to the sign as well as the magnitude of $\vec{M}_{[1\,0\,0]}$. This spread of the Kerr angles might be responsible in parts for the width of the $\Delta\alpha$ peak of MnAs in the frequency-rank distribution.

6. Conclusions

We have studied the optical activity of individual ferromagnetic MnAs clusters embedded in a paramagnetic $In_{0.54}Ga_{0.46}As$:Mn matrix at room temperature by far-field depolarization measurements using a SNOM set-up. The observed optical activity was analyzed in terms of birefringence and Kerr effect and correlated with the structural and magnetic properties of the MnAs clusters determined by FMR measurements. We were able to show that the optical activity of the MnAs clusters in this reflection geometry is almost entirely due to linear birefringence caused by the uniaxial symmetry of the hexagonal crystal structure of MnAs.

Acknowledgements

We are grateful for funding by the Bundesministerium für Bildung und Forschung (BMBF) via contract numbers VDI/EKM 13N6917 and VDI/Spintronics 13N8281 as well as by the Deutsche Forschungsgemeinschaft (DFG) via SFB 484, and project no HE 2298/5-1 and KL 1289/4-1. T.K. was supported by the European graduate college "Electron–electron interactions in solids".

References

[1] J. De Boeck, R. Oesterholt, H. Bender, A. Van Esch, C. Bruynseraede, C. Van Hoof, G. Borghs, J. Magn. Magn. Mater. 156 (1996) 148.
[2] H. Shimizu, M. Miyamura, M. Tanaka, Appl. Phys. Lett. 78 (2001) 1523.
[3] K. Takamura, F. Matsukura, Y. Ohno, H. Ohno, J. Appl. Phys. 89 (2001) 7024.
[4] H. Akinaga, S. Miyanishi, K. Tanaka, W. Van Roy, K. Onodera, Appl. Phys. Lett. 76 (2000) 97.
[5] K. Ando, A. Chiba, H. Tanoue, Appl. Phys. Lett. 73 (1998) 387.
[6] C. Chen, M. Cai, X. Wang, S. Xu, M. Zhang, X. Ding, Y. Sun, J. Appl. Phys. 87 (2000) 5636.

[7] P.J. Wellmann, J.M. Garcia, J.-L. Feng, P.M. Petroff, Appl. Phys. Lett. 71 (1997) 2532.
[8] P.J. Wellmann, J.M. Garcia, J.L. Feng, P.M. Petroff, Appl. Phys. Lett. 73 (1998) 3291.
[9] H. Akinaga, J. De Boeck, G. Borghs, S. Miyanishi, A. Asamitsu, W. Van Roy, Y. Tomioka, L.H. Kuo, Appl. Phys. Lett. 72 (1998) 3368.
[10] D.R. Schmidt, A.G. Petukhov, M. Foygel, J.P. Ibbetson, S.J. Allen, Phys. Rev. Lett. 82 (1999) 823.
[11] M. Mizuguchi, H. Akinaga, K. Ono, M. Oshima, J. Appl. Phys. 87 (2000) 5639.
[12] Y.D. Park, A. Wilson, A.T. Hanbicki, J.E. Mattson, T. Ambrose, G. Spanos, B.T. Jonker, Appl. Phys. Lett. 78 (2001) 2739.
[13] M. Moreno, A. Trampert, B. Jenichen, L. Däweritz, K.H. Ploog, J. Appl. Phys. 92 (2002) 4672.
[14] S. Ye, P.J. Klar, Th. Hartmann, W. Heimbrodt, M. Lampalzer, S. Nau, T. Torunski, W. Stolz, T. Kurz, H.-A. Krug von Nidda, A. Loidl, Appl. Phys. Lett. 83 (2003) 3927.
[15] M. Lampalzer, K. Volz, W. Treutmann, S. Nau, T. Torunski, K. Megges, J. Lorberth, W. Stolz, J. Cryst. Growth 248 (2003) 474.
[16] S. Hara, M. Lampalzer, T. Torunski, K. Volz, W. Treutmann, W. Stolz, J. Cryst. Growth 261 (2004) 330.
[17] H. Shimizu, M. Tanaka, Appl. Phys. Lett. 81 (2002) 5246.
[18] H. Shimizu, M. Tanaka, J. Appl. Phys. 89 (2001) 7281.
[19] P. Fumagalli, A. Rosenberger, G. Eggers, A. Münnemann, N. Held, G. Güntherodt, Appl. Phys. Lett. 72 (1998) 2803.
[20] P. Fumagalli, Adv. Solid State Phys. 39 (1999) 531.
[21] A. Kappitulnik, J.S. Dodge, M.M. Fejer, J. Appl. Phys. 75 (1994) 6872.
[22] P. Bertrand, L. Conin, C. Hermann, G. Lampel, J. Peretti, V.I. Safarov, J. Appl. Phys. 83 (1998) 6834.
[23] B.L. Petersen, A. Bauer, G. Meyer, T. Crecelius, G. Kaindl, Appl. Phys. Lett. 73 (1998) 538.
[24] T. David, C. Chicanne, N. Richard, J.R. Krenn, F. Scheurer, K. Ounadjels, M. Hehn, Y. Lacroute, J.P. Goudonnet, Rev. Sci. Sci. Inst. 70 (1999) 4587.
[25] G. von Freymann, T. Schimmel, M. Wegener, Appl. Phys. A 66 (1998) S939.
[26] G. von Freymann, T. Schimmel, M. Wegener, B. Hanewinkel, A. Knorr, S.W. Koch, Appl. Phys. Lett. 73 (1998) 170.
[27] G. von Freymann, C. Adelmann, G. Scheiber, T. Schimmel, G. Wegener, J. Microsc. 194 (1999) 491.
[28] Th. Hartmann, M. Lampalzer, P.J. Klar, W. Stolz, W. Heimbrodt, H.-A. Krug von Nidda, A. Loidl, L. Svistov, Physica E 13 (2002) 572.
[29] K. Volz, M. Lampalzer, A. Schaper, J. Zweck, W. Stolz, Inst. Phys. Conf. Ser. 169 (2001) 211.
[30] M. Lippitz, M. Schüttler, H. Giessen, M. Born, W.W. Rühle, J. Appl. Phys. 86 (1999) 100.
[32] C.-Y. You, S.-C. Shin, Appl. Phys. Lett. 69 (1996) 1315.
[33] A.M. Stoffel, J. Schneider, J. Appl. Phys. 41 (1970) 1405.
[34] A.G. Bashchikov, A.V. Kimel, R.V. Pisarev, A.A. Rzhevskii, N.S. Sokolov, A. Keen, Th. Rasing, A.M. Nazmul, M. Tanaka, Phys. Solid State 43 (2001) 1941.
[35] F. Iikawa, P.V. Santos, M. Kästner, F. Schippan, L. Däweritz, Phys. Rev. B 65 (2002) 205328.
[36] P. Ravindran, A. Delin, P. James, B. Johansson, J.M. Wills, R. Ahuja, O. Eriksson, Phys. Rev. B 59 (1999) 15680.